Answer to Reviewer 2

We thank Reviewer 2 for their comments. We provide here our responses to those comments and describe how we will address them in the revised manuscript. The original reviewer comments are in normal black font while our answers appear in blue font.

This research project aims to represent the effect of Light-Absorbing Particles (LAP) on snow albedo within the Crocus model as snow aging parameters, and to establish a global climatology of LAP deposition on snow, with the intention of applying these results to land surface models. The effort to achieve a global climatology of this phenomenon, by accounting for the altitude dependence of snow aging and making it regionally specific, is commendable. However, there has been insufficient discussion regarding the methodology for estimating the parameters related to snow aging and LAP climatology when scaling this approach globally. Consequently, it cannot be stated that the reliability of the climatology related to LAP deposition, which is the final outcome, is fully assured. In particular, the following points must be thoroughly discussed:

(major comments)

1. As the author demonstrates, the parameters associated with snow aging show significant differences between the accumulation and melting periods (Fig. 3). However, this study only considered the regional dependency of snow aging. It would be more beneficial for the authors to evaluate snow aging separately for the accumulation and melting periods and then discuss the relationship between snow aging and LAP deposition on the snow. In other words, the climatology of LAP deposition will be influenced not only by altitude but also by the timing of the accumulation and melting periods.

As mentioned by Reviewer 2, Figure 3 in the submitted manuscript shows large changes in the temporal evolution of the simulated albedo with contrasted behavior during the snow accumulation and melting periods. This evolution is mainly explained by four processes simulated by the model:

1. The albedo decrease due to the increase in snow optical grain diameter resulting from dry snow metamorphism during periods without precipitation and no melting. This evolution of the snow optical grain diameter is handled by the metamorphism scheme for dry snow in Crocus (Carmagnola et al., 2014).
2. The albedo decrease due to the increase in snow optical grain diameter resulting from wet snow metamorphism during melting periods. The evolution of the snow optical grain diameter is handled by the metamorphism scheme for wet snow in Crocus (Carmagnola et al., 2014).
3. The albedo decrease in the visible range due to LAP deposition. This effect is empirically represented by the value of gamma in Crocus in the albedo parameterization.
4. The albedo increase due to snowfall which is handled by the snowfall module in Crocus.

The three first processes can be considered as snow aging processes (snow metamorphism and LAP deposition) that are responsible for the decrease of snow albedo with time. However, gamma only directly impacts the third aging process. Therefore, we believe that the term “snow aging coefficient” in the submitted paper was creating confusion for the reader. Reviewer 1 made a similar comment. For this reason, gamma will be renamed the “snow darkening coefficient” in the revised manuscript

since this coefficient is only used to empirically represent the impact of LAP deposition on the snow albedo in the visible range. We believe this new name will help the reader to better understand the role of gamma in the evolution of snow albedo in Crocus. More explanations about the snow albedo parameterization in Crocus will be added to the revised manuscript (Section 2):

The evolution of the optical grain size in Crocus is computed using metamorphism laws as described in Brun et al. (1992) and Carmagnola et al. (2014). For a given layer, for dry snow, the temporal evolution of the optical grain size is a function of the vertical temperature gradient. whereas, for wet snow, the increase in optical grain size with time depends on the snow liquid water content. New snow in Crocus is characterized by an optical diameter of 1e-4 m (surface specific area of 65 m2/kg) and results in an increase in snow albedo.

For the reasons mentioned above, we believe that the snow darkening coefficient should not be too different during the snow accumulation and melting periods since it is not associated with the physical processes that drive the large differences of snow albedo evolution during the accumulation and melting seasons. For example, the impact of the presence of liquid water on the snow optical grain size is handled by the metamorphism scheme in Crocus. Instead, gamma can be seen as an average quantity of LAP in the snowpack. The work proposed in this study allows spatially varying values of gamma based on the climatology of LAP deposition on the snowpack. However, it cannot present the interannual and seasonal variability of LAP deposition on the snowpack. It will be mentioned in the discussion and conclusion of the revised paper:

The methodology developed in this study relies on climatological values of LAP deposition on snow, so that it cannot represent the ***seasonal variation of LAP deposition on snow*** *and the impact of individual LAP deposition events that can strongly influence the evolution of snow albedo (Di Mauro et al., 2015; Dumont et al., 2020).* (Discussion of the revised paper)

This approach takes into account the spatial variability of LAP deposition on snow but cannot represent the seasonal variation of LAP deposition that can result from single deposition events as well as the interannual variability of LAP deposition. (Conclusion of the revised paper)

2. (L173) If the optical thickness of the snow cover is insufficient, the snow albedo will be influenced by the albedo (reflectance) of the ground surface beneath the snow cover. Consequently, γ (gamma) will also reflect the influence of the ground surface. In forested areas, the effect of vegetation must be considered as well. Therefore, γ is not only affected by snow aging but may also be strongly influenced by local factors. It is necessary to provide a comprehensive explanation of this point when determining the relationship between D (climatological deposition rate of LAPs) and γ.

As mentioned in our answer to the first point raised by Reviewer 2, the snow darkening coefficient gamma only represents the effect of LAP deposition on snow albedo in the visible band in Crocus. To avoid the effect of ground contamination on the measurement of snow albedo, a threshold on snow depth has been applied to remove periods when the snow cover was not thick enough. A threshold value of 20 cm was selected for the sites below 60 N and 10 cm was used for the sites above 60 N (L 175-177 of the submitted manuscript). Snow albedo calculations using the online

version of the snow radiative transfer model SNICAR v3 (Flanner et al., 2021) (SNICAR-Online (umich.edu)) have been used to quantify the impact of the ground surface beneath the snow cover on broadband snow albedo for snow depth values corresponding to the threshold values selected in our study. Two snowpack have been considered: (i) a snowpack made of fresh snow with high SSA and low density values (typical of the accumulation season) and (ii) a snowpack made of melt forms with low SSA and high density values (typical of the ablation season). The SSA and density values for each type of snow were taken from Domine et al. (2012). The results are presented in Table 1 below. For a 10-cm (20-cm) thick snowpack made of fresh snow, the ground contamination reduces the snow albedo by 0.8 % (0.2 %). For a 10-cm (20-cm) thick snowpack made of melt forms, the ground contamination reduces the snow albedo by 1.9 % (0.6 %).

Table 1: Snow albedo computed by SNICAR for 2 different snowpack of various thickness.

	Snow albedo values for different snowpack thickness		
Type of snowpack and ground	Thickness = 0.1 m	Thickness = 0.2 m	Thickness = 100 m (optically infinite)
SSA: 65 m2/kg Density: 150 kg/m3 Ground albedo: 0.25 No LAP	0.841090	0.846047	0.848279
SSA: 10 m2/kg Density: 300 kg/m3 Ground albedo 0.25 No LAP	0.772633	0.782954	0.787879

Based on this analysis, we can consider that the threshold values on snow depth applied in this study are sufficient to limit the impact of ground contamination on the snow albedo measurements. This allows us to have a robust comparison between simulated and observed snow albedo and to reduce the potential impact of ground contamination on the optimal ranges of gamma derived at each site. The results of the simulation with SNICAR will be added to the supplementary material. We will also mention these results in the revised paper when describing the criteria imposed to select days for the albedo evaluation:

The first criterion ensured that the observed albedo corresponded to an actual snow albedo value. It made sure that the albedo measurement had been collected over a fully snow-covered ground and that the ground surface beneath the snow cover did not affect the measurement. Observed SD had to be higher than 20 cm. For high-latitude sites (above 60°N), this criterion was relaxed to 10 cm because there is less precipitation at these sites, so SD did not reach far over 20 cm in certain years. Albedo simulations with the radiative transfer model SNICAR v3 (Flanner et al., 2021) confirmed the ground surface beneath the snow cover does not modify the snow albedo by more than 2 % for a 10-cm thick snowpack (see Section xx of the supplementary material)

We fully agree with Reviewer 2 that forest debris from surrounding high vegetation can influence the evolution of snow albedo in the visible range in forested terrain as shown by Melloh et al. (2001). Consequently, gamma should be modified in the presence of high vegetation to represent this effect. The present study focuses only on the large-scale variability of the snow darkening coefficient in open conditions (without trees) as a function of LAP deposition (BC and dust). For this reason, the three forested sites available in the ESM-SnowMIP dataset were not used in this study due to the potential impact of forest debris that could influence the optimal ranges of gamma at these sites as mentioned at L 136-138 in the submitted manuscript. The impact of forest debris on the values of gamma will be included in a new paragraph of the discussion:

In addition, the effects of forest litter and debris on snow albedo in the visible range (Melloh et al., 2001) and on the resulting gamma values were not considered in this study. Only sites located in open terrain were selected to determine the optimal ranges of gamma. Therefore, the values of gamma shown on Fig. 12 do not include the effect of the forest presence. The approach of Hardy et al. (2000) could be considered to indirectly represent the effects of forest litter in the default snow albedo scheme used in Crocus.

3. The climatology of LAP deposition will be a valuable dataset for global land surface models. However, the results presented in Fig. 12 have not been fully validated, and their accuracy, including associated uncertainties, remains unclear. Additionally, because the validation sites are limited, there are likely to be high uncertainties in the LAP data for regions such as South Asia, particularly in mountain glaciers. The authors should release the dataset only after thorough validation.

We agree with Reviewer 2 that the climatology of LAP deposition on snow and the associated values of the snow darkening coefficient are associated with uncertainties. To answer this comment, we will propose two additions to the revised paper:

1. An evaluation of the LAP deposition dataset
2. A quantification of the uncertainty in the values of the snow darkening coefficient resulting from the interannual variability of LAP deposition on snow.

These 2 major additions are described below.

1. A special section describing the accuracy of the GFDL LAP product will be added to the Supplementary material. It will contain a comparison between observed and simulated mean annual dust deposition at 26 sites around the world as shown in Figure 1. The GFDL product captures well the spatial variability of dust deposition around the globe. For example, it reproduces well, the contrasted dust deposition patterns in Central Asia (Fig 1b). For this evaluation, values from 6 different mountain glaciers in Asia have been considered (Table 1). The evaluation of BC climatological deposition is restricted to three sites at the moment as shown in Table 3. It shows that the LAP dataset captures the large differences in BC deposition between the Himalayan mountains and West Antarctica.

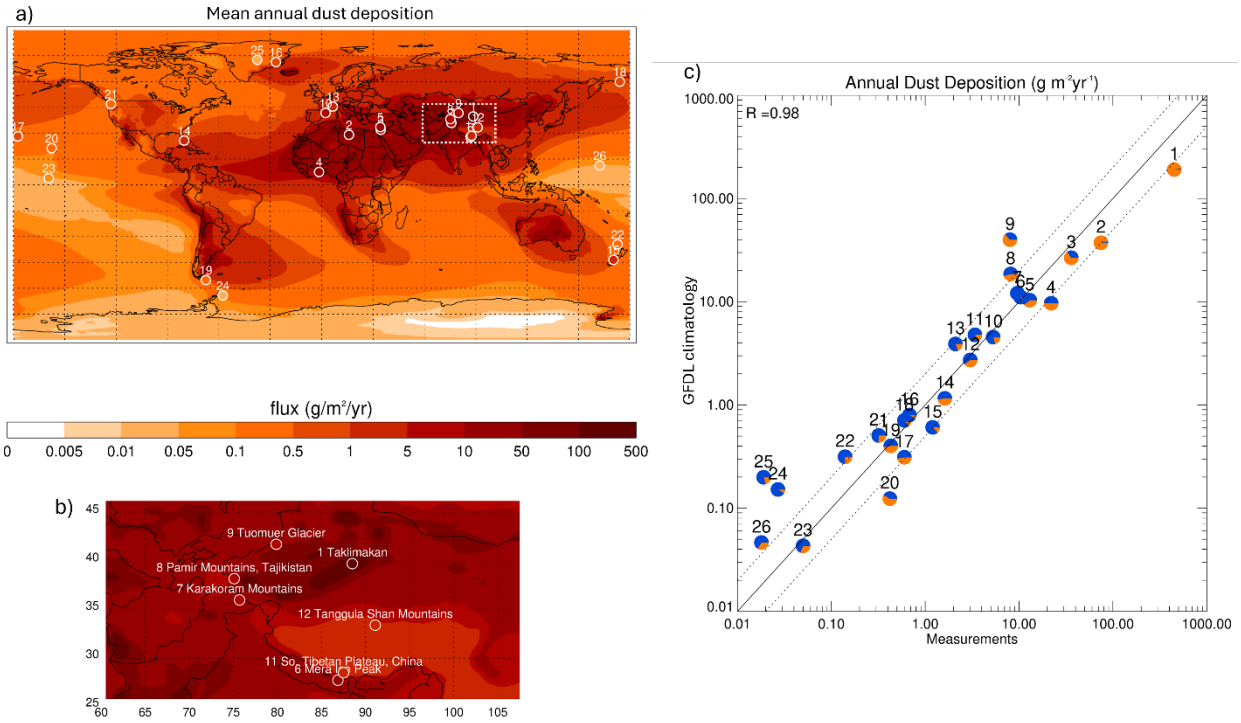

Figure 1 (a) Map showing the mean annual dust deposition from the GFDL climatology (1981-2015), (b) same as (a) for a region centered around the Tibetan Plateau and (c) scatter plot comparing the annual dust deposition in the observation and in the GDFL climatology at 26 sites around the globe. The location of these sites is shown on maps (a) and (b). For each site, the pie chart shows the decomposition in the GFDL climatology between dry (orange) and wet (blue) deposition.

Table 2: Mean annual dust deposition in the observations and in the GFDL climatology at 26 sites. The numbers correspond to the numbers shown on Fig 1.

Num.	Name	Lat.	Lon.	Elev. (m)	Reference	Obs. (g $m^{-2}yr^{-1}$)	Clim. (g $m^{-2}yr^{-1}$
1	Taklimakan	39.75°N	88.50°E	200.	Zhang et al. (1998)	450.00	177.37
2	Waddan	29.12°N	15.93°E	2.	O'Hara et al. (2006)	74.53	34.61
3	Tel Aviv	32.00°N	34.50°E	40.	Ganor and Mamane (1982)	36.00	26.87
4	Ghana, Gulf of Guinea	7.50°N	-1.50°E	0.	Resch et al. (2008)	22.00	9.66
5	Erdemli	33.57°N	34.26°E	21.	Kubilay et al. (2000)	13.00	9.99
6	Mera Ice Peak	27.72°N	86.87°E	6376.	Ginot et al. (2014)	10.40	11.39
7	Karakoram Mtns	36.00°N	75.70°E	5150.	Wake et al. (1994)	9.60	11.28
8	Pamir Mtns	38.20°N	75.10°E	5910.	Wake et al. (1994)	8.14	20.27
9	Tuomuer Glacier	41.75°N	79.87°E	4600.	Zhiwen and Zhongqin (2011)	8.00	31.69
10	Montseny Mtns	41.80°N	2.30°E	700.	Avila et al. (1997)	5.30	4.64
11	So. Tibetan Plateau	28.50°N	87.50°E	5850./6140.	Wake et al. (1994)	3.39	5.28
12	Tanggula Shan Mtns	33.40°N	91.10°E	5950.	Wake et al. (1994)	3.02	2.81
13	French Alps	45.50°N	6.50°E	4270.	Angelisi and Gaudichet (1991)	2.10	3.81
14	Miami	25.75°N	-80.25°E	10.	Prospero et al. (1987)	1.62	1.10
15	Tasman Glacier	-43.50°N	170.30°E	2600.	Windom (1969)	1.20	0.82
16	Renland	71.30°N	-26.70°E	2340.	Bory et al. (2003)	0.68	0.73
17	Midway	28.20°N	-177.35°E	4.	Prospero (1989)	0.60	0.28
18	Shemya	59.92°N	174.00°E	2.	Prospero (1989)	0.60	0.65
19	Navarino Island	-55.22°N	-67.62°E	35.	Sapkota et al. (2007)	0.43	0.53
20	Oahu	21.30°N	-157.60°E	20.	Prospero (1989)	0.42	0.13
21	Mount Olympus	47.00°N	-123.00°E	2000.	Windom (1969)	0.32	0.47
22	New Zealand	-34.50°N	172.75°E	2.	Arimoto et al. (1990)	0.14	0.41
23	Fanning	3.90°N	-159.30°E	25.	Prospero (1989)	0.05	0.04
24	James Ross Island	-64.20°N	-57.70°E	1542.	McConnell et al. (2007)	0.03	0.20
25	GRIP	72.60°N	-37.60°E	3232.	Bory et al. (2003)	0.02	0.18
26	Enewetak	11.30°N	162.30°E	5.	Arimoto et al. (1985)	0.02	0.04

Table 3: Mean annual black carbon deposition in the observations and in the GFDL climatology at three sites.

Num.	Name	Lat.	Lon.	Elev. (m)	Reference	Obs. (g $m^{-2}yr^{-1}$)	Clim. (g $m^{-2}yr^{-1}$)
1	Nepal Clim. Obs.- Pyramid	27.95°N	86.80°E	5079.	Yasunari et al. (2010)	112.00	179.83
2	Tibet Palong-Zanbu Glacier	29.21°N	96.92°E	5500.	Xu et al. (2009)	29.40	77.40
3	West Antarctic Ice Sheet	-79.46°N	-112.08°E	1766.	Bisiaux et al. (2012)	0.02	0.07

2. The impact of the interannual variability of LAP deposition will be considered in the revised version of the manuscript. The GFLD dataset consists of different percentiles (1, 5, 10, 25, 50, 75, 90, 95, 99) of BC and dust deposition rates over the period 1979-2015, for each day of the year. In the submitted paper, the median deposition rate for each day has been considered and combined with the GMASI daily snow cover climatology to obtain an estimation of the mean daily LAP deposition on snow. In

the revised manuscript, we will consider the percentiles 25 and 75 for dust and BC to obtain an estimation of typical daily average LAP deposition on snow for a low LAP year and for a high LAP year. This method provides an estimation of the interannual variability of LAP deposition on snow. The limitations associated with this estimation are mentioned in a paragraph below.

The daily average deposition of dust and BC on snow for a low (high) LAP year will be computed by replacing the median deposition rate by the percentile 25 (75) for each day of the year in Eq. 5 of the submitted paper. The daily average deposition of LAP on snow for a low (high) LAP will be finally expressed in equivalent BC using Eq. 6 of the submitted paper. A coefficient of variability, $C_{v,D}$, will be computed to characterize the inter-annual variability of LAP deposition on snow with respect to the climatology:

$$C_{v,D} = (D_{high} - D_{low})/D_{mean}$$

Where D_{high}, D_{low} and D_{mean} corresponds to the daily average LAP deposition on snow for a high LAP year, a low LAP year and the climatology. Figures 2 and 3 below show how the interannual range LAP deposition on snow ($D_{high} - D_{low}$) and the coefficient of variability, $C_{v,D}$, vary in space. Figure 2 will be added to the supplementary material of the revised paper whereas Figure 3 will be added to the main revised manuscript.

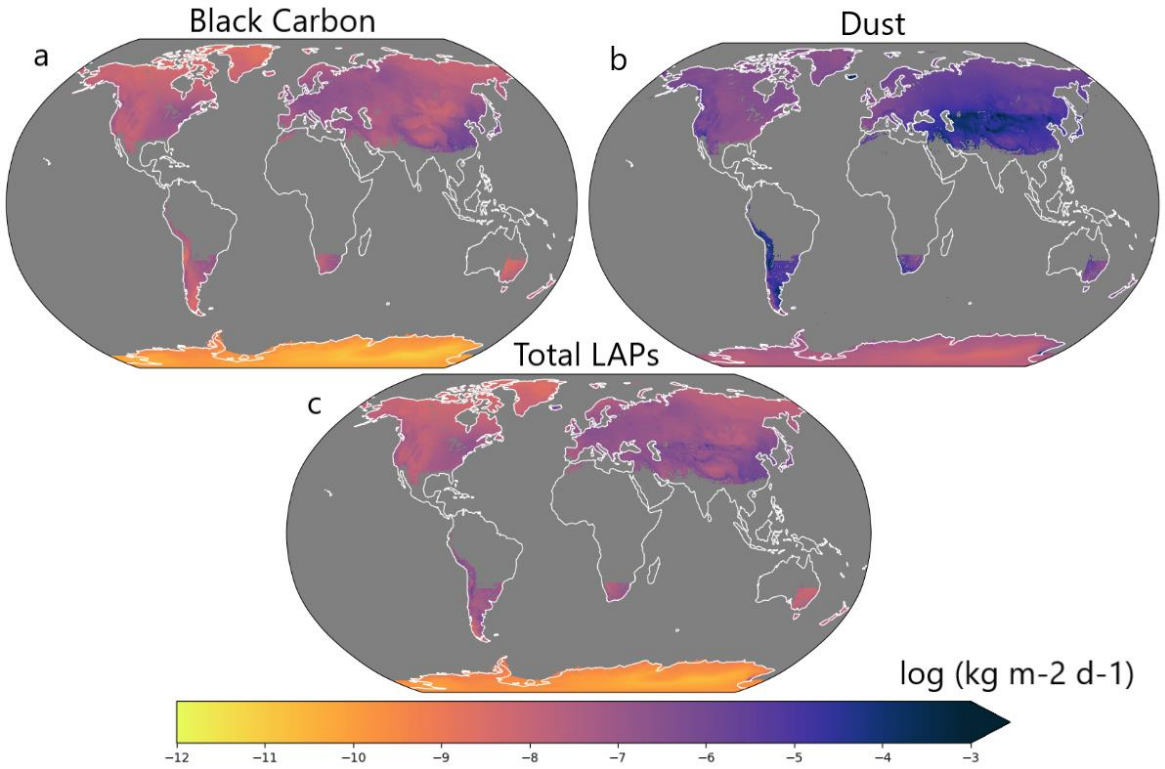

Figure 2: Global maps of the interannual range of daily (a) BC, (b) dust, and (c) total LAP (BC + dust in equivalent BC) deposition rates over snow between a high and a low LAP year ($D_{high} - D_{low}$).

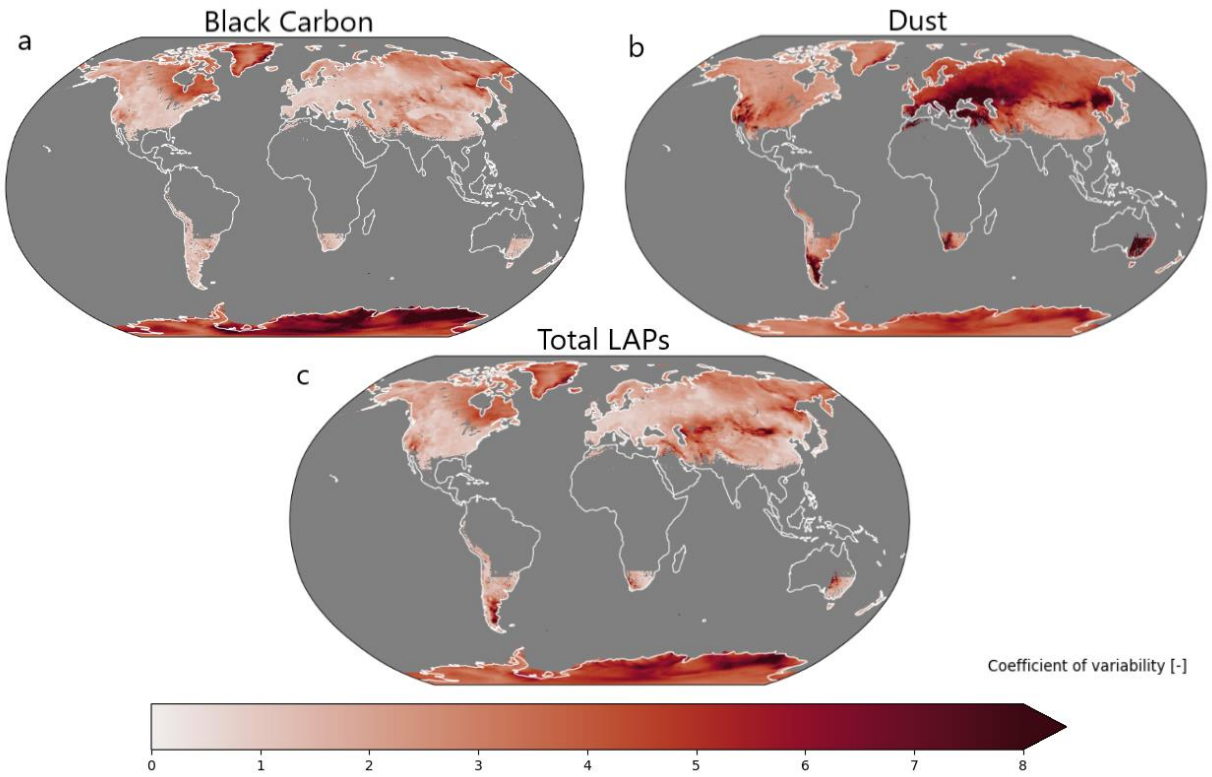

Figure 3: Global maps of the coefficient of variability of daily (a) BC, (b) dust, and (c) total LAP (BC + dust in equivalent BC) deposition rates over snow between a high and a low LAP year.

The LAP deposition rates for a low and a high LAP year will be shown in the cross analysis to illustrate the interannual variability of LAP deposition of snow at each of the experimental sites considered in the study. Figure 9 in the submitted manuscript will be updated to show the interannual variability at all the different sites and the effect of the altitudinal correction (see Fig. 4 below for the revised figure). This figure shows that, despite the interannual variability, sites such as Sapporo or Col de Porte receive significantly larger amounts of LAP on snow than Arctic sites such as Bylot and Umiujaq. The regression between the optimal values of gamma and the climatological LAP deposition on snow at each of the sites won't be modified in the revised manuscript. Indeed, the optimal ranges of gamma at a given site have been selected based on the median RMSE of simulated snow albedo over all the years for each value of gamma. This range is therefore related to the mean climatological LAP deposition on snow at each of the sites. Figure 10 in the submitted manuscript showing the linear regression between gamma and LAP will be updated to show the interannual variability of LAP deposition on snow at each site (see Fig. 4 below for the revised figure).

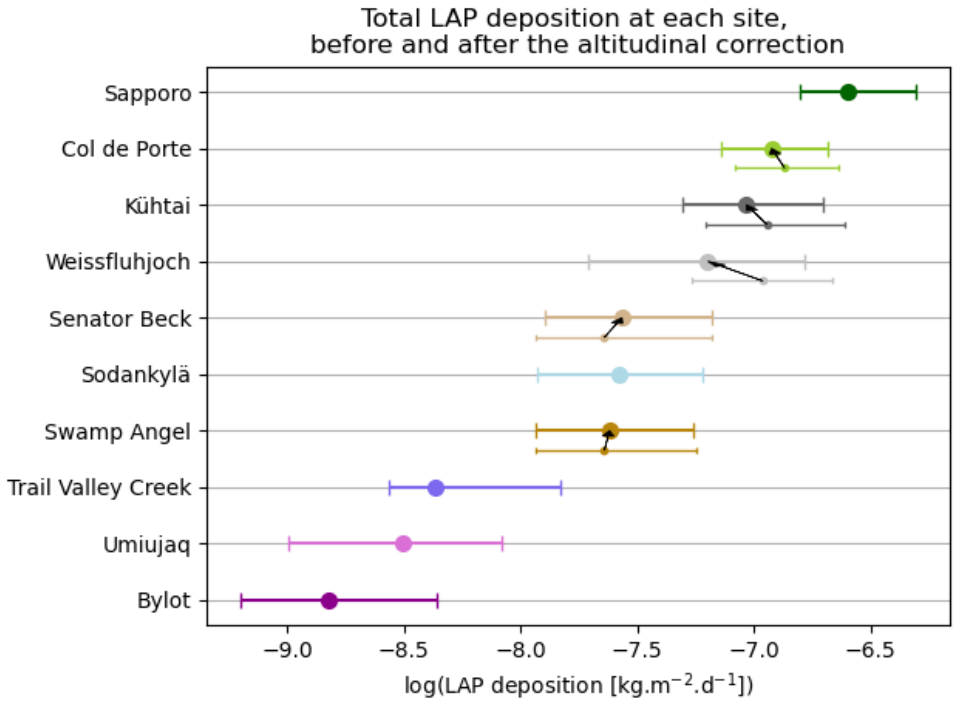

Figure 4: Graph representing climatological LAP deposition rates at all sites, before and after the correction of elevation effects. Arrows indicate these corrections at mountainous sites. The error bar represents the interannual variability of LAP deposition at each site.

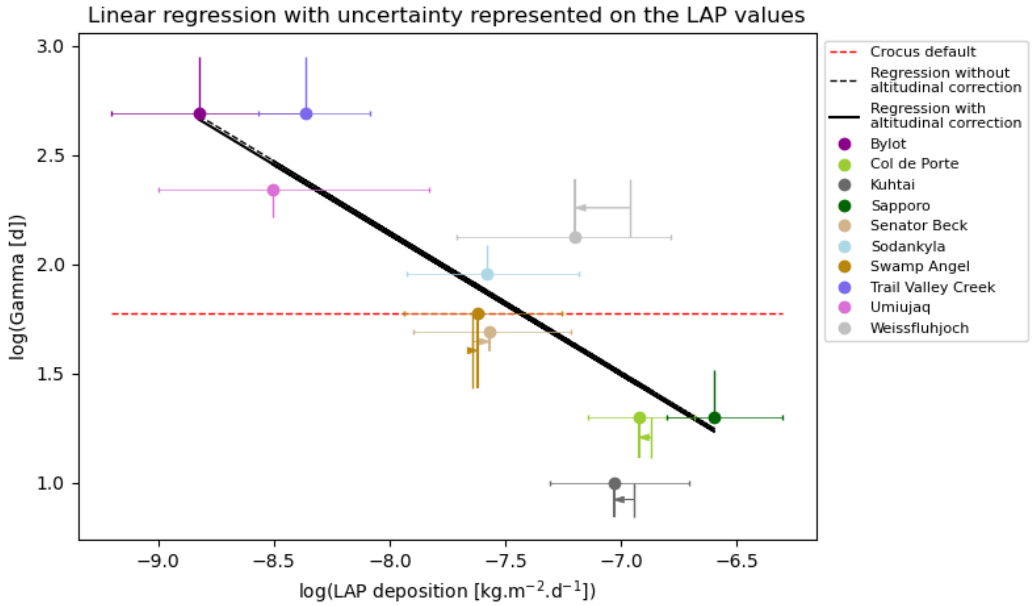

Figure 5: Graph representing the optimal ranges of γ as a function of total LAP deposition rates in equivalent BC, in logarithmic scales, and the corresponding linear regressions with and without correction for elevation at the mountain sites (the correction is represented by the arrows). The error bar represents the interannual variability of LAP deposition at each site.

The estimation of the interannual variability of LAP deposition on snow is calculated for a low LAP year and a high LAP year using the percentiles 25 and 75 for dust and BC deposition available in the GFDL dataset. Such a method can only provide an estimation of interannual variability. A more accurate computation would have required to use the deposition rates of BC and dust for each day of the period 1979-2015 in the GDFL dataset and to combine them with the corresponding GMASI snow cover information. Mean daily deposition of LAP on snow could have then been computed for each year of the climatology and the interannual variability could have been estimated precisely. Unfortunately, the daily LAP deposition data were not available in the version of the GFDL dataset used in this study. Future work could use these daily data once they are available or use another source of global LAP deposition data at daily time scale such as the MERRA-2 dataset. These limitations will be mentioned in the discussion of the revised manuscript.

The values D_{high} and D_{low} for dust, BC and total LAP will be added to the dataset distributed on Zenodo. This will provide the users of the climatology of LAP deposition on snow with an estimation of the interannual variability of LAP deposition on snow.

The uncertainty in the estimation of gamma resulting from the interannual variability of LAP deposition on snow will be quantified in the revised paper. We propose to account for this uncertainty in the revised paper by computing the values of gamma corresponding to a low LAP year and to a high LAP year using the regression given in Eq. 9 of the original paper and the map of LAP deposition on snow for a low LAP and high LAP year. Similarly to the coefficient of variability computed for the LAP deposition on snow, we propose to compute a coefficient of variability for the value of gamma:

$$C_{v,\gamma} = (\gamma_{high} - \gamma_{low})/\gamma_{mean}$$

Figure 12 in the submitted paper will be updated to add a map that shows how $C_{v,\gamma}$ varies globally (see Fig. 6 below). The largest uncertainties for gamma are found in regions where the interannual variability of LAP deposition on snow is the largest. This includes the east coast of North America and central Siberia that are close to regions of BC emissions. The Karakum Desert, the Aral Sea and the Gobi Desert are also regions of large variability in gamma due to the strong interannual variability of dust deposition in these regions. Finally, Antarctica shows no interannual variability of gamma since the gamma values for the low and high years are equal to 900 days (the maximal value allowed for gamma in Crocus) due to very low LAP deposition on snow.

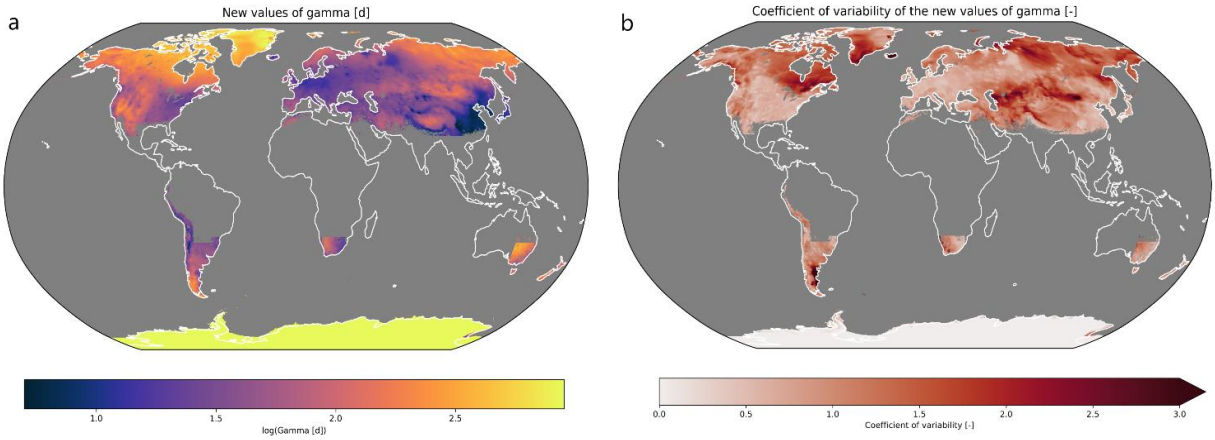

Figure 6: Global maps showing (a) the optimal value of γ derived and (b) the associated uncertainty due to the LAP interannual variability.

The values γ_{high} and γ_{low} will be added to the dataset distributed on Zenodo. This will allow the users of the model to know where the values of gamma are uncertain due to the interannual variability of LAP deposition on snow. Such uncertainty could be considered in the context of ensemble snowpack simulations.

(minor comments)

1. It is understood that Crocus is a multi-layer model used to simulate snow conditions across various layers. However, only two snow grain size parameters (d_opt and d') are employed to calculate the albedo in the visible and near-infrared regions (Table 1). In the visible range, ice exhibits weak light absorption, allowing light to penetrate more deeply. Therefore, to accurately calculate the albedo in the visible range, it is crucial to consider the vertical distribution of snow grain sizes. Please add an explanation of which snowpack layer d_opt parameter represents.

Thanks for this comment. We agree with Reviewer 2 that the description of how Crocus handles solar radiation was not sufficient in the submitted manuscript. We will add the following information about the model. First, the snow albedo in Crocus is computed as a depth-weighted average of the albedo of the two upper snow layers, so on a total depth of a few to a tens of cm. The properties (d_opt, age) of each layer are used to compute their respective albedo. This method is applied to avoid time discontinuities in the simulated snow albedo resulting from layer aggregation. Second, Crocus simulates the penetration of incoming shortwave radiation into the snowpack and its absorption assuming an exponential decay of radiation with increasing snow depth. The absorption coefficient in the different spectral bands depends on the optical diameter and on the density of each snow layer.

The following sentences will be added to the revised paper:

The snow albedo in each band is obtained as a depth-weighted average of the albedo of the two upper snow layers. The properties (d_opt, age) of each layer are used to compute their respective albedo. This method is applied to avoid time discontinuities in the simulated snow albedo resulting from layer aggregation.

Crocus simulates the penetration of incoming shortwave radiation into the snowpack and its absorption assuming an exponential decay of radiation with increasing snow depth. The absorption coefficient in the different spectral bands (Table 1) depends on the optical diameter and on the density of each snow layer.

Table 1 in the paper will be revised to include the snow absorption coefficient for each band as shown below:

Table 1. Equations representing the snow albedo and the snow absorption coefficient for the three spectral bands in Crocus. The parameters are as follows: d_{opt} (m) is the optical grain diameter of the snow, ρ the snow density, P (Pa) is the mean pressure at the site, P_{CDP} (Pa) is the mean pressure at the Col de Porte site, A (days) is the age of the snow, and γ (days) is the snow ~~aging~~ darkening coefficient. Adapted from Table 4 in Vionnet et al. (2012).

Spectral band	Spectral albedo $\alpha_{spectral\ band}$	Absorption coefficient β (m^{-1})
0.3—0.8 µm	$\alpha_{0.3-0.8\mu m} = \max(0.6, \alpha_i - \Delta\alpha_{age})$ $where: \alpha_i = \min(0.92, 0.96 - 1.58\sqrt{d_{opt}})$ $and: \Delta\alpha_{age} = \min(1, \max(\frac{P}{P_{CDP}}, 0.5)) \times 0.2\frac{A}{\gamma}$	$\beta_{0.3-0.8\mu m} = \max(40, 0.00192\frac{\rho}{\sqrt{d_{opt}}})$
0.8—1.5 µm	$\alpha_{0.8-1.5\mu m} = \max(0.3, 0.9 - 15.4\sqrt{d_{opt}})$	$\beta_{0.8-1.5\mu m} = \max(100, 0.01098\frac{\rho}{\sqrt{d_{opt}}})$
1.5—2.8 µm	$\alpha_{1.5-2.8\mu m} = 346.3d' - 32.31\sqrt{d'} + 0.88$ $where: d' = \min(d_{opt}, 0.0023)$	$\beta_{1.5-2.8\mu m} = +\infty$

2. Please explain how the solar zenith angle dependence of snow albedo and the effects of the atmosphere, especially clouds, on snow albedo can be expressed in terms of Eq. 1.

The dependence of snow albedo on the solar zenith angle and the influence of the cloud cover and optical thickness on the distribution of the incoming radiation in the three spectral bands is not considered in the default albedo scheme in Crocus. This limitation will be explicitly mentioned in the revised manuscript when detailing the snow albedo parameterization in Crocus:

The model does not include the change in the ratio of incoming radiation in the three bands as a function of the sky conditions and of the solar zenith angle. The impact of these limitations is discussed in Sect. 5.

We will then discuss the uncertainties associated with these limitations in the discussion of the revised paper:

Despite the improvements brought in this study, the default snow albedo in Crocus still suffers from limitations associated with the fixed ratio used to compute the broadband albedo from the values in the three spectral bands (Eq. 1) and the absence of effect of the solar zenith angle on snow albedo. Gardner and Sharp (2010) have shown that changes in solar zenith angle and clouds' optical

thickness can lead to changes on the order of 0.05 in the snow albedo values (Fig. 9 in their study). Including these effects will lead to further improvements in large scale snow albedo simulations with Crocus.

3. For reference, please also show the results for SSA=10 m^2kg^-1 (~granular snow) in Fig. 1.

The two figures below show how the snow albedo decrease with snow age varies as a function of the snow darkening coefficient gamma for two values of SSA (50 m^2 kg^{-1} as in the submitted paper and 10 m^2 kg^{-1} as suggested by Reviewer 2). In the visible range (Figure 2), the two graphics are identical since the reference albedo value for a snow age of 0 is equal to 0.92 for both values of SSA (see Table 1 in the main manuscript). On the other hand, the two SSA values lead to different albedo values in the two near-infrared bands so that for a given age and a given value of gamma, the broadband albedo is lower for SSA = 10 m^2 kg^{-1} than for SSA = 50 m^2 kg^{-1}.

We have decided to keep unchanged Figure 1 in the revised manuscript since the two values of SSA give the same albedo evolution as a function of snow age in the visible range.

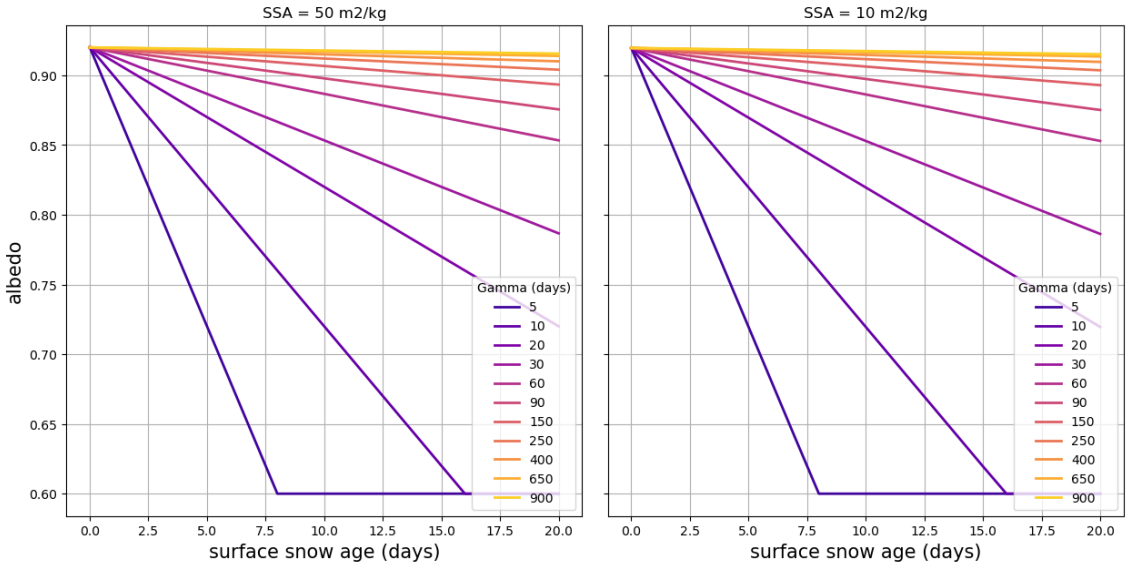

Figure 6 Graphic representation of the dependency of the snow albedo in the visible spectral band (0.3–0.8 µm) to the snow age for different values of gamma and for two SSA values (50 m2/kg and 10 m2/kg)

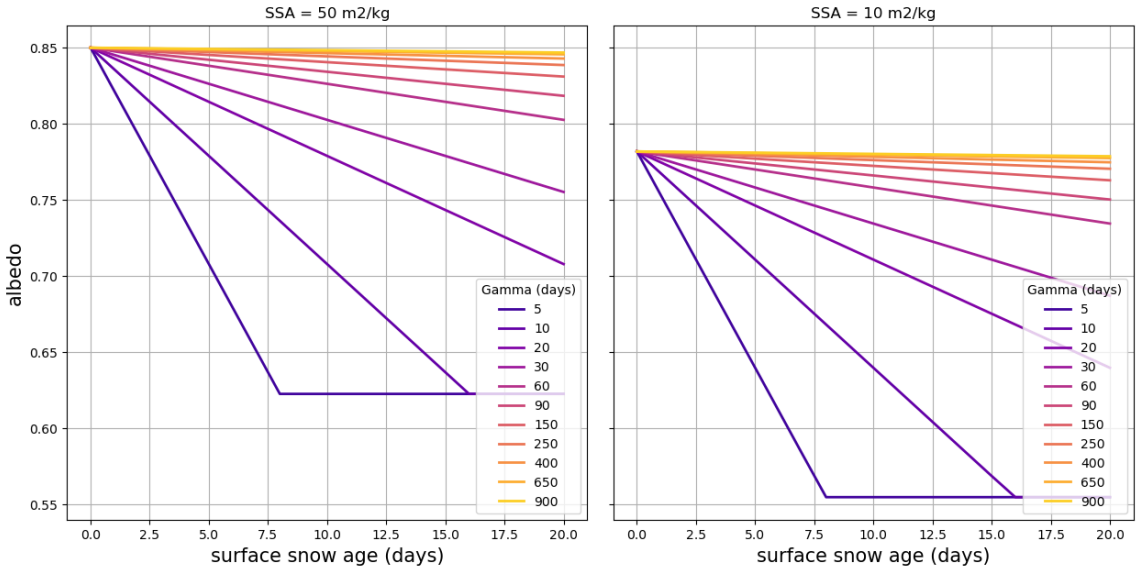

Figure 7 Graphic representation of the dependency of the broadband snow albedo (0.3−0.8µm) to the snow age for different values of gamma and for two SSA values (50 m2/kg and 10 m2/kg)